Journal of Information Systems and Telecommunication
Vol.11, No.2, January-March 2023, 75-83
http://jist.acecr.org
ISSN 2322-1437 / EISSN:2345-2773

Broadband Low-cost Reflectarray based on a New Phase Synthesis Technique and a Class of Cross Bow-tie Cells

Mahmood Rafaei-Booket[1*], Mahdieh Bozorgi[1], Seyed Mostafa Mousavi[2]

[1].Department of Electrical and Computer Engineering, University of Zanjan, Zanjan, Iran
[2].Missouri University of Science and Technology, USA

Received: 30 Nov 2021/ Revised: 04 Jun 2022 / Accepted: 05 Jul 2022

Abstract

In this paper, a class of Bow-tie unit cell on FR4 substrate is designed and investigated to be used in implementing a single-layer broadband Reflectarray Antenna (RA). In the analyzing step, two different parameters (length and angle) of the grounded Cross Bow-Tie (CBT) are varied to obtain the phase diagrams. Various degrees of freedom in the CBT structure are very helpful in designing a broadband RA. In the antenna design procedure, an efficient phase synthesis technique is applied to minimize the adverse effects of frequency dispersion causing by the differential space phase delay at different frequencies. This technique optimizes the metallic CBTs arrangement on the aperture of RA, and reduces the dependency of RA design to the CBT's phase variation. Consequently, combination of the CBT's phase behavior and the phase synthesis technique leads to designing a broadband RA with a good frequency response. In addition to, the Side Lobe Level (SLL) of the resultant RA is reduced remarkably. For validation of the obtained numerical results, an RA is designed and fabricated in 8.7~12.3GHz frequency bandwidth. The measurements show 27.03 dB as a maximum gain value at 10.2 GHz with a 1.5dB gain bandwidth of 34%. It is also shown that the implemented RA exhibits a reduced SLL (<-18dBi) within its operating bandwidth.

Keywords: Reflectarray; Cross Bow-tie unit cell; Broadband Antenna; Phase Synthesis Method; Low-cost structure.

1- Introduction

The Reflectarray Antennas (RAs) are a suitable alternative for phased array antennas, and conventional reflectors in military applications, space telecommunication, and remote sensing. The considerable deployment RAs is due to their exceptional features such as lightness, compactness, and flexibility of controlling radiation pattern. In addition, the use of RAs eliminates the need for expensive and complex custom molds, making RAs affordable [1]. Meanwhile, the narrow bandwidth of RAs is their main disadvantage. The narrow bandwidth of their unit cell and differential spatial phase delay lead to achieving their narrow bandwidth performance [1-3]. For solving this problem, wideband unit cells are designed with the help of periodic substrate [4], stacked patches [5], anisotropic substrates [6-9], and complex unit cells [10, 11]. Although the use of multilayer unit cells can increase the phase ranges and operating bandwidth of RAs [12], on the other hand, the weight, loss, complexity, and manufacturing cost of RAs increase. To address this deficiency, two different solutions have been described in the literature. The first solution is based on designing a wide phase range unit cell that is performed by a trial-and-error technique. Such a technique is a time-consuming and tedious one and leads to complex and multilayer unit cells [10-12]. The alternative solution is to use the optimization technique described in [13]. This optimization technique minimizes the phase realization errors of each element at center and two extreme frequencies within working bandwidth. Although the latter technique is beneficial, the various metallic elements' error function values in the array do not have a clear relationship in the optimization procedure. This results in local minima, which in turn results in sub-optimal frequency performance of the antenna.

To design a broadband RA, this paper first presents a method for minimizing the adverse effects of the frequency dispersion. This method is a new phase synthesis technique to achieve an appropriate arrangement

✉ **Mahmood Rafaei-Booket**
Booket@znu.ac.ir

of elements on RA's aperture and thereby a broadband RA. Then, a single-layer unit cell consisting of sub-wavelength metal Cross Bow-Tie (CBT) elements on a grounded low-cost substrate is proposed. The low-cost substrate is considered to be thick FR4. Using such a thick lossy substrate needs a tradeoff between reducing the insertion loss of the unit cell and optimizing the reflected power [14, 15]. Simulation results show that the reflectivity of the proposed class of CBT unit cell is so remarkable. Moreover, additional freedom degree of such a unit cell in comparison to cross-dipole [4] increases the phase range, which is needed to design broadband RAs. The obtained reflection information of the under-study unit cell is then applied for designing a planar center-fed RA. The design by means of the mentioned phase synthesis technique leads to obtaining the most appropriate metallic CBTs arrangement on the aperture of RA. As a result, the operation bandwidth of the designed single-layer RA is increased and Side Lobe Level (|SLL|) of its radiation pattern is reduced in comparison to the described traditional method in [13]. Such a technique is thoroughly examined with experimental demonstration and the designed center-fed RA is fabricated and measured in X-band (8.7~12.3GHz).

2- A Technique for Selecting Optimum Arrangement of RA Design

In RA designing, the proper phase distribution on its aperture is the main step such a way that the realized phases have a minimum deviation from the calculated phase distribution in the working frequencies. Based on [1], for designing an RA with a single pencil-beam in (θ_b, φ_b), the required phase shift of the i^{th} element located in (x_i, y_i) point is given by:

$$\phi_R = k_0 \left(d_i - \left(x_i \cos\varphi_b + y_i \sin\varphi_b \right) \sin\theta_b \right) \quad (1)$$

that, the length of path from horn antenna's phase center to i^{th} element on the array indicated by d_i. obviously, satisfying the relation (1) is quite easy for RA design in a single frequency. However, it becomes more difficult to meet this requirement in each frequency sample once the working bandwidth of RA is increased, and the designer is faced with more phase realization errors. Such errors are mainly due to the differential spatial phase delay factor as mentioned in [1]. To control the behavior of the antenna in the desired bandwidth, an optimization technique is proposed in [13] and an optimal element arrangement on the aperture of RA is achieved by minimizing the error function defined as follows:

$$e(m,n) = \sum_{i=l,c,u} \left| \Phi^{\text{desired}}(f_i)(m,n) - \Phi^{\text{achieved}}(f_i)(m,n) \right| \quad (2)$$

Where (m,n) refer to a particular location on RA lattice and $\Phi_{f_i}^{\text{desired}}(m,n)$ and $\Phi_{f_i}^{\text{achieved}}(m,n)$ represent desired and achievable phase delays at given frequencies (l, c, and u represent lower, center, and upper frequencies, respectively). This procedure first calculates the phase distributions that meet the requirements of the mask in the center and the two extreme frequencies. In the second step, the most appropriate element is selected to minimize the error function at each element of RA lattice regardless of the other elements. The lack of a relationship between error function values in [13] leads to a local minimum in the optimization procedure. To explain further, in this method, the value of the error function for one element may be close to zero, while the value for the neighboring element may be large, resulting in suboptimal antenna performance. Solving this problem, an optimization technique is used that minimizes the average of the error function values calculated for all RA elements [8].

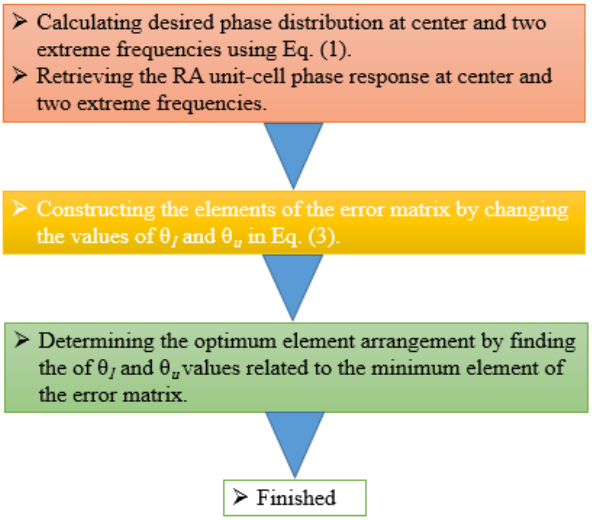

Fig. 1 Block chart of the introduced phase synthesis method.

For more explanation our phase synthesis method, suppose that the "$[\Phi]$" is the calculated phase shifts on the aperture of RA and "θ" is an arbitrary and a constant phase. In this case, "$[\Phi]+\theta$" leads to the identical radiation pattern. This property helps the designer to have freedom degrees in phase shifts distribution realizing with a minimum error and thereby attain an RA with optimum performance. To this end, the total phase error of the entire array is taken into account and the mentioned error function in (2) is modified as follows:

$$e(\theta_l,\theta_u)=\min\left\{\sum_{m,n}\left[\begin{array}{l}\left|\Phi_{f_l}^{\text{desired}}(m,n)-\Phi_{f_l}^{\text{achieved}}(m,n)+\theta_l\right|+\\ \left|\Phi_{f_c}^{\text{desired}}(m,n)-\Phi_{f_c}^{\text{achieved}}(m,n)\right|+\\ \left|\Phi_{f_u}^{\text{desired}}(m,n)-\Phi_{f_u}^{\text{achieved}}(m,n)+\theta_u\right|\end{array}\right]\times w(m,n)\right\} \quad (3)$$

for all members of the search space

and for $\theta_l=-180:\text{step}:180$ and $\theta_u=-180:\text{step}:180$

The relation of (13) is an objective function that needs to be calculated for database of different RA element's classes. It should be noted that the smaller the step in (3), the smaller the error, but a step of 1 degree or less does not significantly affect the antenna performance. On the other hand, the second principle is incorporated into (3) as a weighting function, $w(m,n)$, where elements closer to the center of the RA surface are given higher weights and elements closer to the RA edge are given lower weights. Thus, $e(\theta_l,\theta_u)$ is the best arrangement of RA cells minimizing (2). The structural information of the optimal elements of the RA is then automatically determined by selecting the arrangement that minimizes the error matrix.

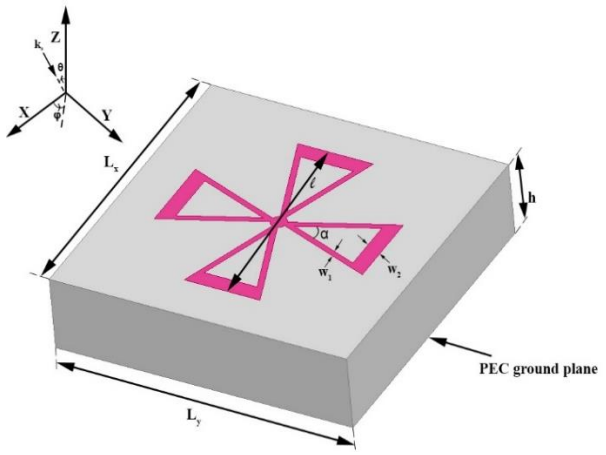

Fig. 2 Geometry of grounded CBT unit cell with FR4 substrate used for planar RA design.

Fig. 1 is a block diagram summarizing the phase synthesis technique introduced.

3- Element Design

Herein, the CBT unit cell is proposed inspiring from the bow-tie antenna structure. Its sketch and design parameters have been shown in Fig. 2. As shown in this figure, the reflected wave of CBT is affected by changing its length (l) and angle (α). In this case, the metallic array is printed on a grounded FR4 substrate with ε_r=4.4 and loss tangent δ_c=0.02 as a low-cost dielectric. In [15], analyzing a single-layer unit cell with FR4 dielectric, it was found that the utilizing of a thick lossy dielectric (FR4) results in low loss in respect to a thin one. Thus, the thickness of FR4 substrate has been chosen h=2.4mm. In addition, the period of lattice is considered to be smaller than $\lambda/2$ for designing a wideband RA [16]. The use of unit cells with smaller sizes leads to lower sensitivity to the angle of incident wave and improves the assumption of the infinite periodic structure. Meanwhile, (l /L_x) must be selected to achieve sufficient linear phase range for an RA designing. In this regard, L_x=L_y=0.35λ in the central frequency 10.5GHz, and 0.2<l/L_x<1 means the elements are sub-wavelength to achieve a maximum linear phase range [17]. The other parameters of CBT unit cell are optimized as: L_x=L_y=10mm, W_1=0.3mm, and W_2=0.9mm. In order to analyze the proposed unit cell and investigate the effects of the lossy substrate on the reflection characteristics, a common practice is adopted, where the element is assumed to be surrounded by an infinite periodic array of the same cells [1]. Such a simplification is called the local periodicity assumption which is validated by good agreement between theoretical RA design and its measurements [4].

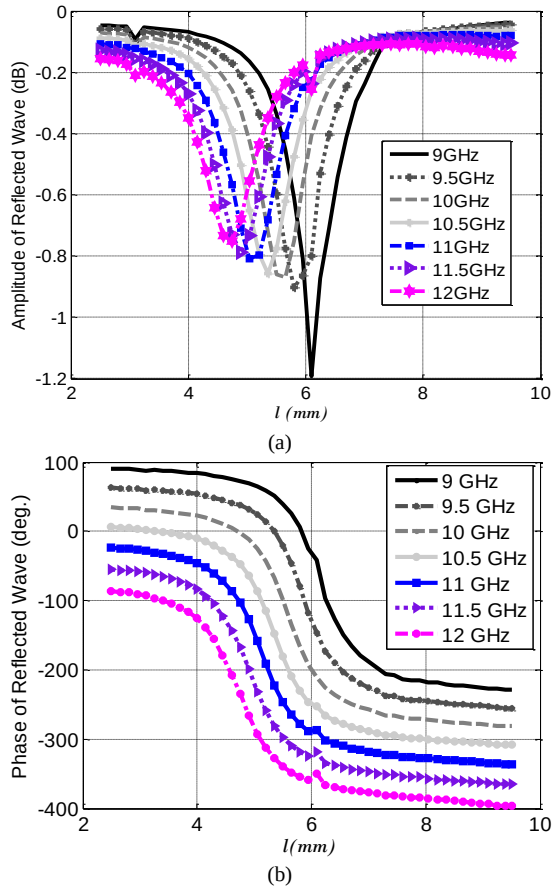

Fig. 3 Amplitude, and (b) phase diagrams of CBT unit cell versus of l variations (α=30°).

Table 1: Parameters of RA element for different classes

W_1 (mm)	W_2 (mm)	α(degree)	*l*(mm)
0.1~0.5	0.1~0.9	30°~80°	2.4-9.6
Step: 0.05	Step: 0.05	Step: 1°	Step: 0.2

Therefore, the full-wave analysis of the proposed CBT with periodic boundary conditions is carried out by means of a Finite Element Method (FEM)-based EM-solver. The reflection information of such a unit cell illuminated by a normally plane-wave is calculated in 9~12GHz frequency range, as shown in Fig. 3. The amplitude diagram is shown in Fig. 3(a) to estimate the unit cell loss. In Fig. 3(b), the phase responses are obtained versus of the element's length (*l*) variations. In these cases, the angle α=30°. To increase the phase range, the element length is left unchanged in its maximum value (*l* = 9.6mm) and the phase response is recalculated by means of the angle (α) variations from 30° to 80°. This range for angle α is allowable due to CBT's geometry.

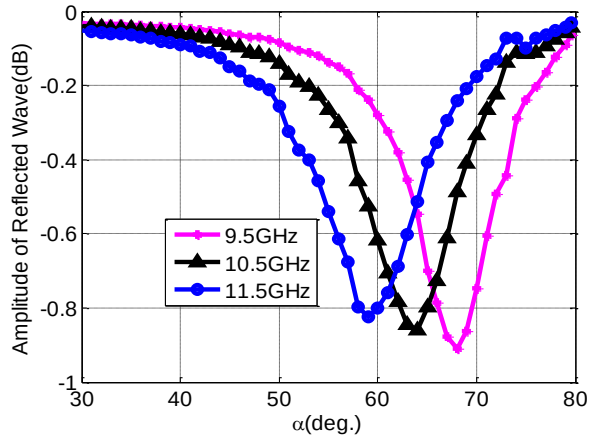

(a)

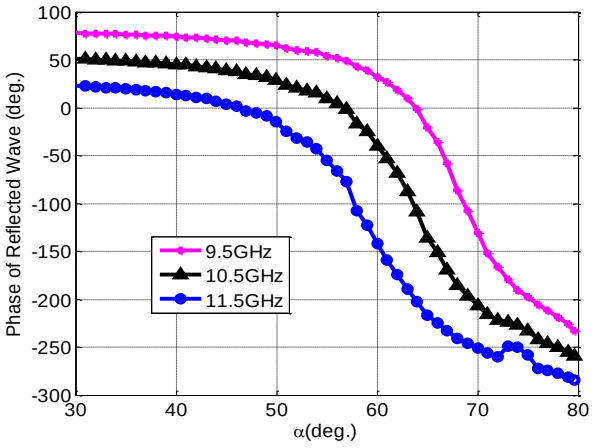

(b)

Fig. 4 Amplitude, and (b) phase diagrams of CBT unit cell versus of α variations (*l*=9.6mm).

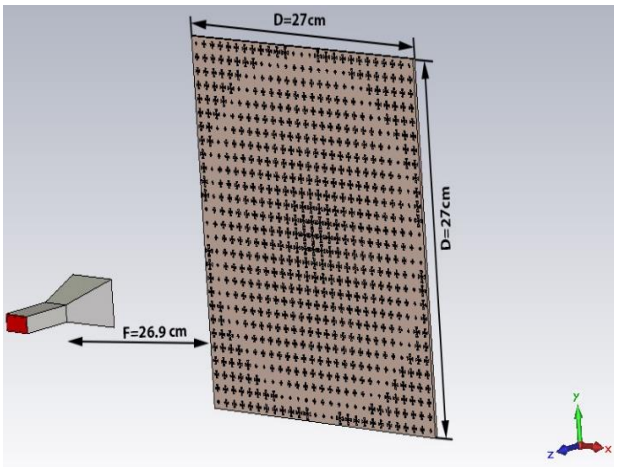

Fig. 5 Simulated RA and its feed antenna.

The reflected wave information versus variation of the angle α is visualized in Fig. 4. As shown in Fig. 4(b), another phase response with an approximately linear phase response is obtained in 9~12GHz.

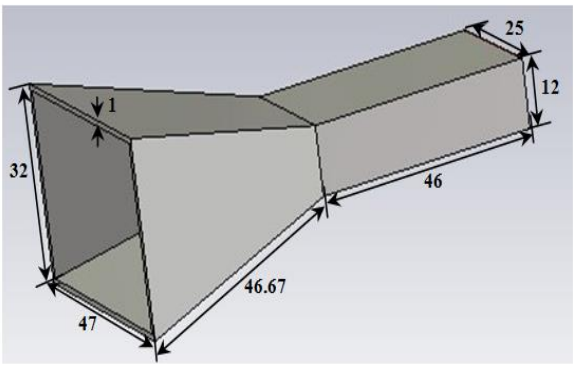

(a)

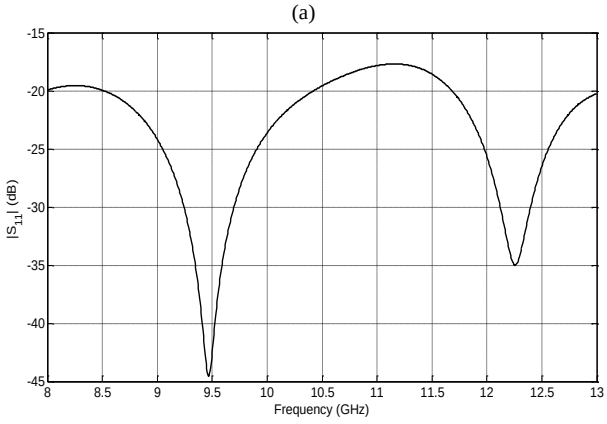

(b)

Fig. 6 (a) Simulated horn antenna and its dimensions vs. mm, and (b) its impedance matching curve [25].

This demonstrates that the proposed element has an additional freedom degree to obtain a wider phase range

than cross-dipole element [4]. Fig. 3(a) and Fig. 4(a) show that, the average reflectivity of the unit cell with thick lossy substrate is close to 0dB for operating frequencies. This leads to the selection of the best values for α and *l* to reduce the sensitivity of the phase diagram in RA implementation. Various unit cell's classes have been obtained by varying W_1, W_2, *l* and α in Fig. 1. The different structural variations to make the phase response database are indicated in Table 1. The obtained phase and amplitude diagrams are used in the following to design a center-fed RA by means of the presented phase synthesis technique in block diagram of Fig. 1.

4- Optimum Broadband RA Design and Experimental Verification

In order to justify the effectiveness and practicality of the described optimization method, and proposed unit cell in Sec. 2, and Sec. 3, respectively, a low-cost single-layer RA is designed and manufactured in X-band having a very wide bandwidth. In this case, the calculated phase diagrams of the unit cell in Fig. 3(b) and Fig. 4(b) are used. In order to find the best performing element configuration at the RA frequency using the introduced phase synthesis technique, a database containing the unit cells' phase responses for all permutations was separately generated at the center (10.5 GHz) and at the two extreme frequencies (9GHz, and 12GHz). In these frequencies, the needed phase shift for each cell of RA aperture must be evaluated. To this end, one can use the method described in [1].

The corresponding equivalent elements' dimensions (*l* and α) are thus determined from the resultant phase diagrams (Fig. 3(b), and Fig. 4(b)) with the minimum error. In this regard, the center-fed RA depicted in Fig. 5 is simulated. As it is shown in the same figure, the planar array includes 27×27 CBT elements illuminated by a horn antenna. Since in center-fed RAs, feed blockage has its own role in the reducing the system efficiency, we have designed a horn antenna with small aperture size ($3.2\times4.7cm^2$) to decrease the effect of feed blockage. Its dimensions and schematic of the simulated horn are depicted in Fig. 6(a). Its return loss diagram is shown in Fig. 6(b) and indicates that the horn antenna works within the desired RA bandwidth. Moreover, the horn antenna's radiation patterns in H- and E-planes are respectively visualized in Fig. 7(a), and Fig. 7(b). In these patterns, Half Power Beam Width (HPBW) of the designed horn is 41° for H-plane and 46.5° for E-plane patterns, respectively. Its peak gain value is 13.3dBi at 10.5GHz. Thus, the exponent of feed pattern function represented by $\cos^q\theta$ is q=4.72, which is used in the RA design. Since the dimensions of center-fed RA is $27\times27cm^2$, the focal length (horn antenna's phase center) is calculated 26.9cm to maximize the antenna efficiency. According to the calculated phase diagrams, the required phase shifts of 27×27 elements of this center-fed RA are calculated and shown in Fig. 8. For such an RA, the half of the subtended angle from the aperture of RA to the horn antenna's phase center (θ_e) is 27.7°. The phase diagram is calculated assuming that a normal incident plane wave irradiates all the RA's elements, but it is clear that such an assumption will reduce the overall gain and decrease the antenna efficiency. Therefore, the angular dependency of the phase diagrams is also taking into account. For this purpose, the phase diagrams in terms of $l(\alpha=30^o)$, and $\alpha(l=9.6mm)$ are recalculated for different oblique incident angles in the central frequency. As shown in Fig. 9, the little dependences of phase variations on the incident angle are observed once the incident θ is less than θ_e. Additionally, for avoiding the grating lobe in the radiation pattern, the element spacing in RA (L_x, L_y) must follow the array equation [18]:

$$L_x, L_y \le \frac{\lambda_0}{(1+\sin\theta_{inc})} \quad (4)$$

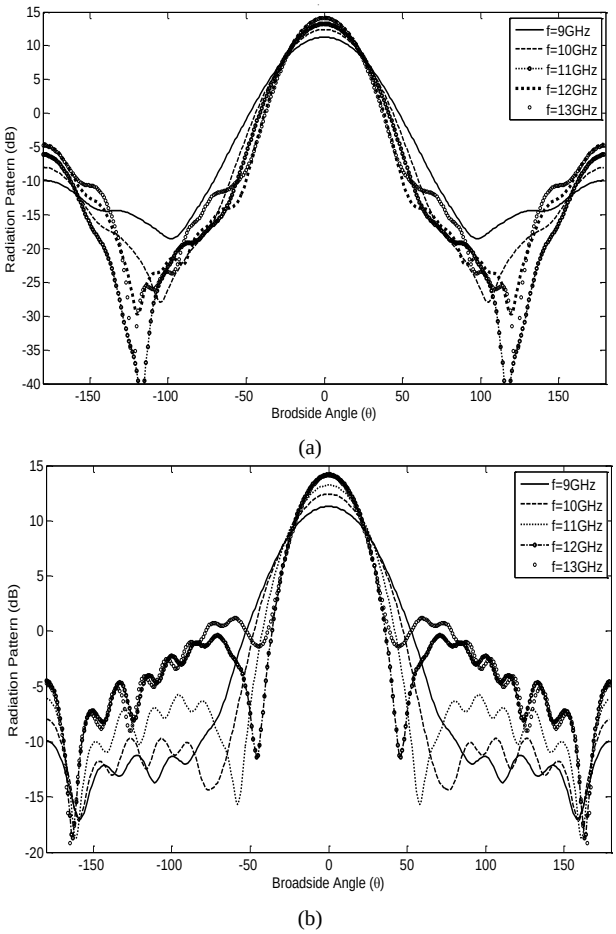

Fig. 7 Radiation patterns of the simulated horn antenna in (a) H-, (b) E-planes in frequency range 9~13GHz.

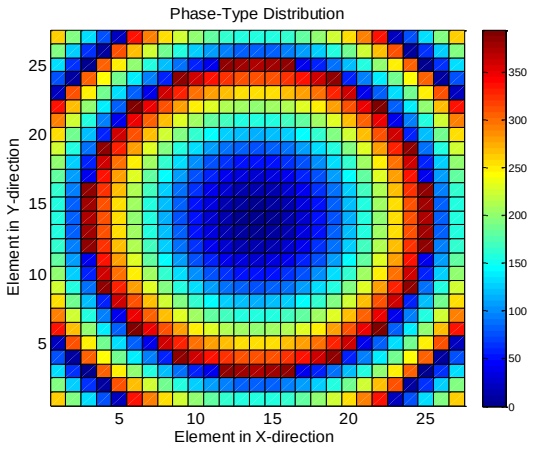

Fig. 8 The elements' phase shifts required in designing a center-fed RA with 27×27cells.

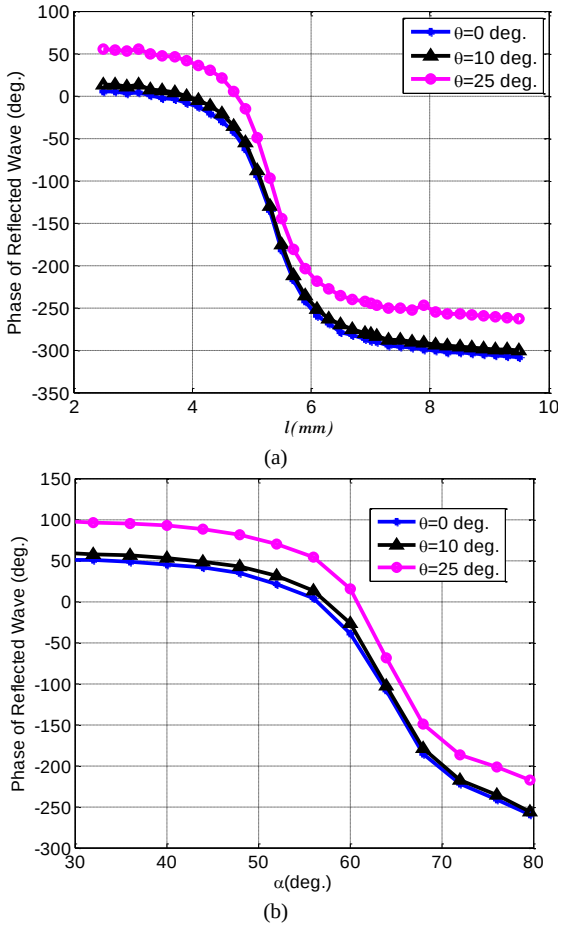

Fig. 9 Phase variations of the proposed CBT at central frequency 10.5GHz for various oblique incidences (θ_{inc} is the incident angle) when (a) l, and (b) α are changed.

in which, λ_0 is the free-space wavelength, and the incident angle θ_{inc} is less than θ_e. The unit cell's dimensions satisfy limitation of (4) due to $L_x = L_y$ =10mm=0.35λ_0. For really assessment of the introduced phase synthesis technique, the analytically calculated radiation patterns in H- and E-planes at 10.5GHz are respectively visualized in Fig. 10(a), and Fig. 10(b). In these figures, the radiation patterns calculated using the common approach [13] are observed. These figures show that our phase realization technique allows a lower SLL than the common one. Choosing the proper elements and reducing the error of RA's phase synthesis leads to the mentioned SLL reduction. It should be pointed out that the average error of the phase realization is decreased from 40° in [13] to 5° on each RA's element. The antenna structure including RA surface along with its horn antenna is simulated using an EM-solver and its surface current distribution is obtained at 10.75GHz, as shown in Fig. 11.

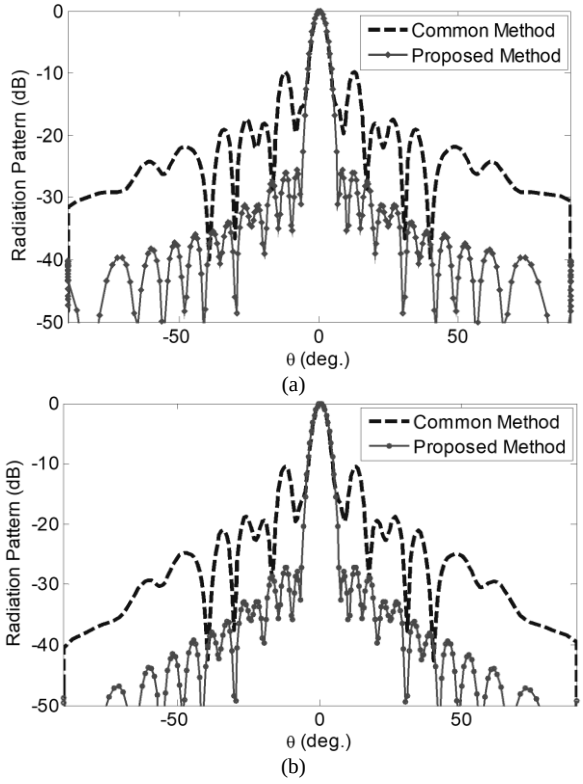

Fig. 10 Analytical radiation patterns at 10.5GHz, (a) H-plane, and (b) E-plane which are obtained by the RA aperture's phase distribution realized using the CBTs. The calculated radiation patterns by means of traditional method [13] are reported for comparison.

To validate the obtained numerical results, the designed system is fabricated. The photo of this low-cost implemented RA on FR4 substrate is observed in Fig. 12. The simulated radiation patterns and measured ones in E-, and H-plane at 10.2GHz are shown in Fig. 13(a), and 13(b), respectively. Measured Cross-polar radiation patterns are indicated by red dashed-lines in these figures.

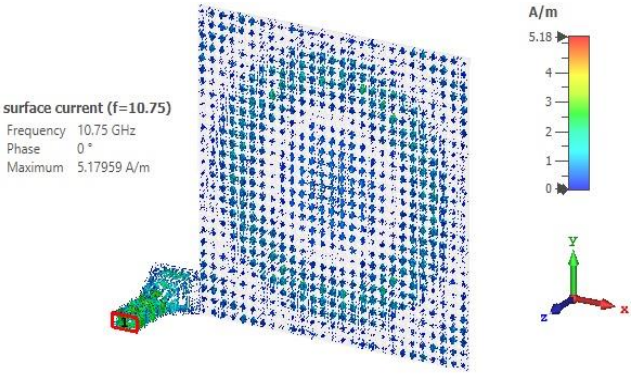

Fig. 11 Simulated current distribution of the designed RA.

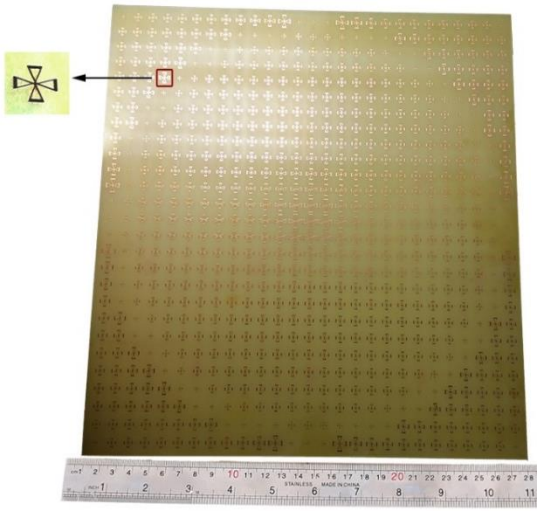

(a)

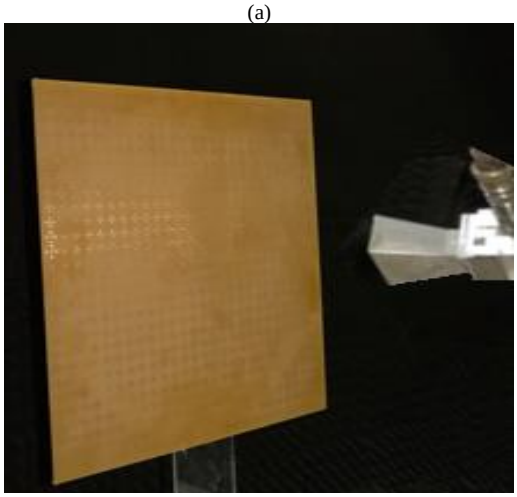

(b)

Fig. 12 Fabricated RA, (a) its photo from up view, and (b) RA along with horn antenna in anechoic chamber.

Also, the measured |SLL|<-18dB. Fig. 14 demonstrates the simulated and measured peak gain values versus frequency. As seen in the same figure, the maximum gain of the implemented RA is 27.03dB at 10.2GHz and its 1.5dB bandwidth of about 34% (8.7~12.3GHz) is achieved. Note that the goal of this study is not to design a high gain RA. However, a phase realization technique is introduced to broaden the RA's bandwidth and reduce its |SLL|. Obviously, if the number of array's cells and dimension of RA aperture are increased, the gain of the resultant structure can be enhanced. In some reported single-layer RAs like that [22], an air layer was added between dielectric and ground layer for gain enhancement.

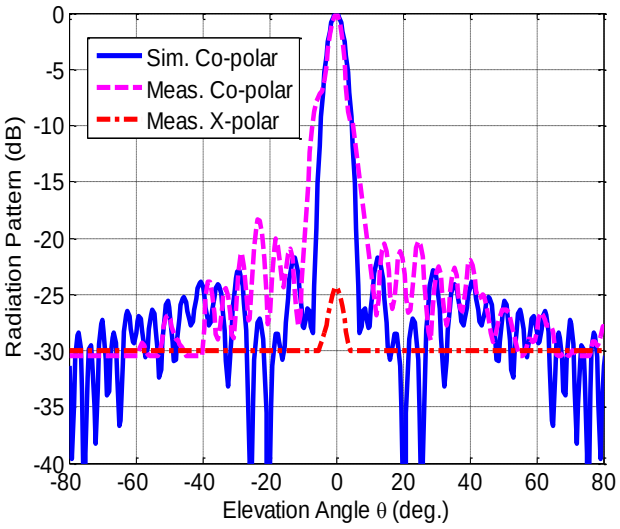

(a)

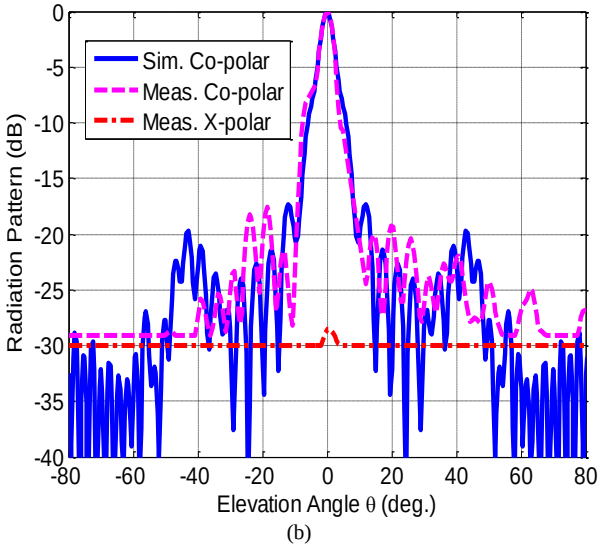

(b)

Fig. 13 Normalized radiation patterns of the implemented RA at 10.2GHz in (a) E-plane, and (b) H-plane.

The comparison results of Table 2 confirm that a satisfactorily trade-off between bandwidth and |SLL| is obtained by combination of our optimization technique and proposed CBT unit cell. The maximum efficiency for such a system can be given by:

$$\eta_{total} = \lambda_0^2 \frac{G_{\max}}{4\pi A} \times 100, \quad (5)$$

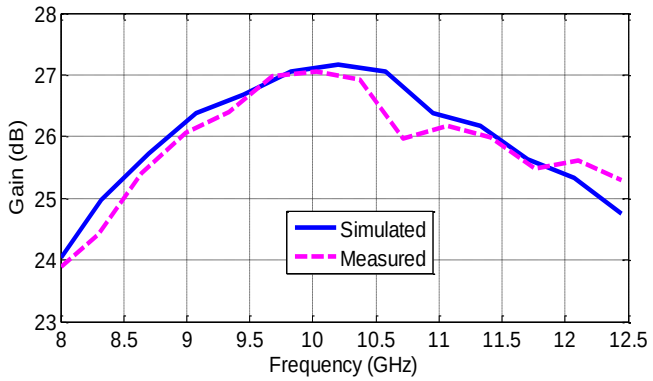

Fig. 13 Measured and simulated peak gain values of the implemented RA.

TABLE 2: Comparison of the Single-layer RAs

Ref.	Dim. of array (cm)	Cells No.	Freq. range (GHz)	G_{max} (dB)@ f_c	BW (%)	Max. phase range (deg.)	|SLL| (dB) @ f_c
[19]	40 ×40	1225	12.5 ~14.5	34.0	16.7	360	<-14
[20]	27×19	650	10.7 ~12.5	25.3	9.7	480	<-14
[21]	25×25	625	10.0 ~11.2	25.4	12	700	<-12
[13]	120×120	10000	11.4 ~12.8	40.6	11.6	400	<-16
[4]	27×27	729	8.95 ~12.1	26.57	29.5	400	<-14
[22]	Dia.=30	988	8.7 ~10.7	27.7	25	450	<-15
This Work	**27×27**	**729**	**8.7 ~12.3**	**27.03**	**34**	**610**	**<-18**

where G_{max} is the measured maximum gain (= 27.03dB) at 10.2GHz, and A is the RA's aperture area (=0.27×0.27m^2). Thus, the total efficiency is obtained 48%.

In Table 3, its estimated efficiencies and losses are summarized. As shown in the same table, the blockage of horn antenna is in the order of unit cell loss. It should be noted that the feed loss does not include loss in the transmission line between the horn antenna and transceiver. Therefore, one can obviously use an offset-fed design for increasing the RA efficiency.

TABLE 3: Estimated efficiency of the implemented low-cost broadband RA

Type	Efficiency (%)	Loss (dB)
Illumination	85	0.7
Spillover	72	1.42
Unit cell	91	0.41
Cross-pol [23]	95	0.22
Feed antenna [24]	91	0.41
Total	48	3.16

5- Conclusions

A metal cross bow-tied array on a thick lossy grounded FR4 dielectric is presented to implement a broadband, low-cost and single-layer RA. It is shown that presented unit cell with bow-tie patch layer gives us more phase range due to its two different design parameters (its length and angle). The obtained phase diagrams of this unit cell are used for implementation of an RA with 27×27 elements in X-band. Measured results indicate the implemented RA provides a gain of 27.03dB with a variation of less than 1.5dB over a relative gain-bandwidth of 34% (8.7~12.3GHz) and |SLL|<-18dB at 10.2GHz, which is an excellent performance compared with other single layer RAs designed in X-band. This feature is the result of using a robust phase realization technique, taking wave incident angle on each RA element into account and benefiting from a large database of RA elements.

References

[1] J. Huang, and J. A. Encinar, Reflectarray Antennas, Hoboken. NJ: John Wiley & Sons, 2008.

[2] D. M. Pozar, "Bandwidth of reflectarrays,", Electron Lett., Vol. 39, No. 21, 2003, pp. 1490-1490.

[3] M. Rafaei-Booket, and Z. Atlasbaf, "New Ku-band reflectarray antenna by using anisotropic superstrate on an artificial magnetic conductor," International Journal of Microwave and Wireless Technologies, Vol. 9, 2016, pp. 831-841.

[4] M. Rafaei-Booket, Z. Atlasbaf, and M. Shahabadi, "Broadband reflectarray antenna on a periodically perforated substrate," IEEE Trans. Antennas Propag., Vol. 64, No. 8, 2016, pp. 3711-3717.

[5] J. A. Encinar, and J. A. Zornoza, "Three-layer printed Reflectarrays for contoured beam space applications," IEEE Trans. Antennas Propag., Vol. 52, No. 5, 2004, pp. 1138-1148.

[6] M. Rafaei-Booket, and Z. Atlasbaf, "Metallic grating embedded in an anisotropic slab for realization of a reflectarray antenna," In 23th Iranian Conference on Electrical Engineering (ICEE), 2015, pp. 10-14.

[7] M. Bozorgi, and M. Rafaei-Booket, "Metallic array on a biased Ferrite substrate as a reflectarray antenna," In 9th International Symposium on Telecommunications (IST), 2018, pp. 80-85.

[8] M. Rafaei-Booket, and S. M. Mousavi, "Efficient analysis method and design approach for broadband reflectarrays with

isotropic/-artificial anisotropic substrates," IET Microwaves, Antennas & Propag., Vol. 14, No. 10, 2020, pp. 1108-1116.
[9] X. Li, Y. Wan, J. Liu, D. Jiang, T. Bai, K. Zhu, J. Zhuang, and W.-Q. Wang, "Broadband electronically scanned reflectarray antenna with liquid crystals," IEEE Antennas and Wireless Lett., Vol. 20, No. 3, 2021, pp. 396-400.
[10] E. Carrasco, M. Barba, and J. A. Encinar, "Reflectarray element based on aperture-coupled patches with slots and lines of variable length," IEEE Trans. Antennas Propag., Vol. 52, No. 3, 2007, pp. 820-825.
[11] E. Carrasco, J. A. Encinar, and M. Barba, "Bandwidth improvement in large Reflectarrays by using true-time delay," IEEE Trans. Antennas Propag., Vol. 56, No. 8, 2008, pp. 2496-2503.
[12] E. Ozturk, and B. Saka, "Multilayer Minkowski reflectarray antenna with improved phase performance," IEEE Trans. Antennas Propag., 2021, DOI: 10.1109/TAP.2021.3090533.
[13] M. R. Chaharmir, J. Shaker, N. Gagnon, and D. Lee, "Design of broadband, single layer dual band large reflectarray using multi open loop elements," IEEE Trans. Antennas Propag., Vol. 58, No. 9, 2010, pp. 2875-2883.
[14] H. Rajagopalan, and Y. Rahmat-Samii, "On the reflection characteristics of a reflectarray element with low-loss and high-loss substrates," IEEE Trans. Antennas Propag., Vol. 52, No. 4, 2010, pp. 73-85.
[15] F. Costa, and A. Monorchio, "Closed-form analysis of reflection losses in microstrip reflectarray antennas," IEEE Trans. Antennas Propag., Vol. 60, No. 10, 2012, pp. 4650-4660.
[16] J. Ethier, M. R. Chaharmir, and J. Shaker, "Loss reduction in reflectarray designs using sub-wavelength coupled-resonant elements," IEEE Trans. Antennas Propag., Vol. 60, No. 11, 2012, pp. 5456-5459.
[17] P. Nayeri, F. Yang, and A. Z. Elsherbani, "Braodband reflectarray antennas using double-layer subwavelength patch elements," IEEE Antennas Propag. Lett., Vol. 9, 2010, pp. 1139-1142.
[18] M. Bozorgi, and Z. Atlasbaf, "Spectral solution for scattering analysis of periodic plasmonic nano-antennas on iso/-anisotropic substrate," J. Lightwave Technol., Vol. 34, No. 11, 2016, pp. 2624-2630.
[19] Y. Mao, Sh. Xu, F. Yang, and A. Z. Elsherbani, "A novel phase synthesis approach for wideband reflectarray design," IEEE Trans. Antennas Propag., Vol. 63, No. 9, 2015, pp. 4189-4193.
[20] H. Hasani, M. Kamyab, and A. Mirkamali, "Low cross-polarization reflectarray antenna," IEEE Trans. Antennas Propag., Vol. 59, No. 5, 2011, pp. 1752-1756.
[21] M. Maddahali, and K. Forooraghi, "High efficiency reflectarray using smooth tapering in phase pattern on antenna surface," Microwave and Optical Lett.,Vol. 55, No. 4, 2013, pp. 747-753.
[22] R. S. Malfajani, and B. A. Arand, "Dual-band orthogonally polarized single layer reflectarray antenna," IEEE Trans. Antennas Propag., Vol. 65, No. 11, 2017, pp. 6145-6150.
[23] J. Huang, "Analysis of a microstrip reflectarray antenna for micro- spacecraft application," TDA Progress Report, 1995.
[24] C. A. Balanis, Antenna Theory: Analysis and Design, 3rd ed. John Wiley & Sons; 2005.
[25] M. Rafaei-Booket, and M. Bozorgi, "Low-cost inhomogeneous material for low-RCS reflectarray antenna implementation," AEU- International Journal of Electronics and Communications, Vol. 149, 2022, pp. 154182.